Supplementary: Silicon vacancy center in 4H-SiC: Electronic structure and spin-photon interfaces

Ö. O. Soykal,[1] Pratibha Dev,[1,2] and Sophia E. Economou[3,4]

[1] *NAS-NRC fellow residing at Naval Research Laboratory, Washington, DC 20375, USA*
[2] *Department of Physics and Astronomy, Howard University, Washington, DC 20059, USA*
[3] *Naval Research Laboratory, Washington, DC 20375, USA*
[4] *Department of Physics, Virginia Tech, Blacksburg, Virginia 24061, USA*

SINGLE PARTICLE MOLECULAR ORBITALS

General remarks

Unlike the case of NV center in diamond, and other similar defects such as the axial divacancy in SiC, although we expect the single charged Si vacancy to still have a $C_{3\nu}$ symmetry, it can still be interpreted as a very weakly broken T_d symmetry. This is because all four nearest neighbors to the vacancy are carbon atoms with very similar distances (differing by $\sim$1%) from the nearest silicon atom in a perfect crystal, and we do not expect this qualitative feature to change much upon removal of the silicon atom. We thus anticipate that the form of A_1 symmetry molecular orbitals will be very close to those of T_d:

$$\begin{aligned} u^{T_d} &= a + b + c + d, \\ v^{T_d} &= a + b + c - 3d, \end{aligned} \tag{1}$$

where the normalization has been omitted for brevity. Based on the 'nearly-T_d' symmetry we also anticipate that state v will be near-degenerate with states e (in T_d they are degenerate). As we show below, our single-particle molecular orbitals obtained using DFT indeed confirm these qualitative expectations. Combining results from DFT with analytical calculations we can derive further information, such as the coefficients in the molecular orbitals, overlap integrals and on-site Coulomb energies.

First principles calculations

In order to complement the main group theoretic results, density functional theory (DFT) was used to obtain single particle molecular orbitals (MOs) of the charged Si-vacancy center in 4H-SiC. The ordering of the defect states is obtained from the calculated Kohn-Sham eigenstates around the bandgap of 4H-SiC. The spin-polarized calculations were carried out using the Quantum-ESPRESSO package [1], within the generalized gradient approximation (GGA) [2] of Perdew-Burke-Ernzerhof (PBE) [3]. In this work, we report the results for the V_{Si}^{-1} at the h-site in a $6 \times 6 \times 2$ (576-atoms) supercell with Γ-centered $2 \times 2 \times 2$ k-point sampling according to Monkhort-Pack method. The large size of the supercell considered here ensures a reduction in the defect-defect interactions. This produces nearly-flat defect states that are labeled as $u/\bar{u}$ (A_1-symmetry), $v/\bar{v}$ (A_1-symmetry)and $e/\bar{e}$ (E-symmetry). Here, the letters with bar overhead represent the minority spin state, with the excess of three-electrons in the majority spin states. The MOs of the defect plotted in Figure 1 differ from those obtained with group theoretic methods (using symmetry-adapted sp^3-orbitals) in that they are not restricted to the dangling bonds only. In DFT-calculations no such restriction is made and it includes contributions from other electronic states of the crystal as well. Nonetheless, the defect states can be seen to be highly localized on the carbon atoms surrounding the defect. The majority spin u, is found to be resonant with the valence band, while the higher energy defect-states lie in the band gap. This ordering of the defect states can be seen in Fig.2. Thus, the DFT-results reproduce the correct symmetries expected from the group theoretic results and provide the ordering of the defect states relative to each other. In the main text we used

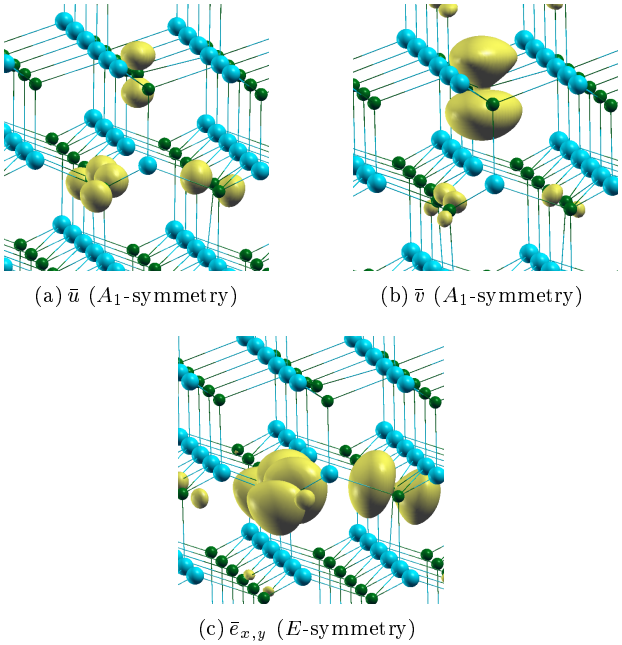

(a) $\bar{u}$ (A_1-symmetry) (b) $\bar{v}$ (A_1-symmetry)

(c) $\bar{e}_{x,y}$ (E-symmetry)

FIG. 1. (color online) Isosurface plots ($5 \times 10^{-3} e/a.u^{-3}$) for the optically-active minority spin MOs of the negatively charged silicon vacancy center V_{Si}^{-} in 4H-SiC: (a) the highest occupied orbital, $\bar{u}$, (b) the lowest unoccupied orbital, $\bar{v}$, and (c) the next higher unoccupied orbital, $\bar{e}_{x,y}$.

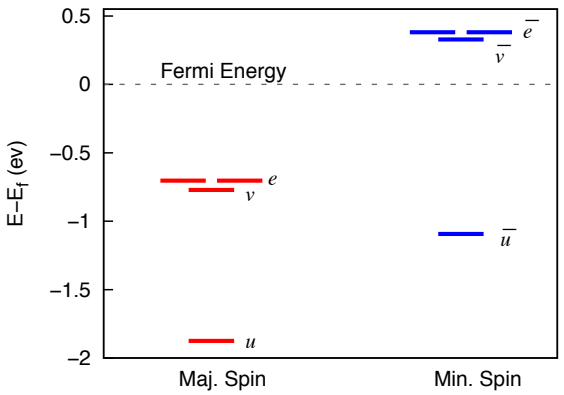

FIG. 2. The energy ordering of the defect-induced majority- and minority-spin states.

group-theoretic approach to obtain single-particle MOs from the symmetry-adapted linear combinations of the sp^3-orbitals belonging to the four carbons surrounding the silicon vacancy. However, group theory does not yield the relative ordering of states with same symmetry, which can be obtained from the DFT calculations. In Fig.3, we choose a different isosurface (compared to the isosurface plots in Fig.1) to showcase the bonding- and the anti-bonding characters of the A_1 symmetry states u and v, respectively. Thus, DFT results can be used to shed light on the relative ordering of the MOs qualitatively (bonding vs. anti-bonding) and quantitatively (Fig.2).

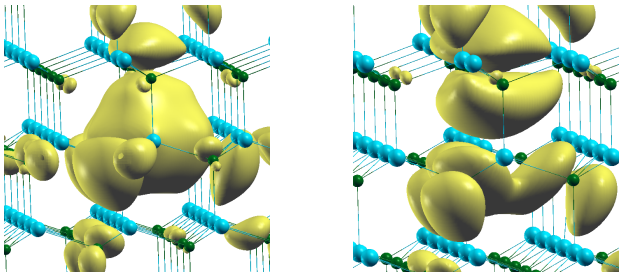

(a) $\bar{u}$ (A_1-symmetry) (b) $\bar{v}$ (A_1-symmetry)

FIG. 3. (color online) Isosurface plots ($5 \times 10^{-4} e/a.u^{-3}$) for the optically-active minority spin MOs with A_1-symmetry, showing: (a) bonding character of u, and (b) anti-bonding character of v.

Coulomb interaction and overlap integrals

The Coulomb interaction Hamiltonian can be grouped as $V_c = \sum_{i\neq j} v_{ij} + \sum_i v_{ii}$ in terms of interactions between different sites (denoted by ij) and on-site (ii) interactions. Therefore, the Schrödinger equation in the basis of sp^3 dangling bonds [4] takes the form of

$$\begin{pmatrix} v_{aa} & v_{ab} & v_{ab} & v_{ad} \\ v_{ab} & v_{aa} & v_{ab} & v_{ad} \\ v_{ab} & v_{ab} & v_{aa} & v_{ad} \\ v_{ab} & v_{ab} & v_{ab} & v_{dd} \end{pmatrix} = E_n \begin{pmatrix} 1 & \lambda_1 & \lambda_1 & \lambda_2 \\ \lambda_1 & 1 & \lambda_1 & \lambda_2 \\ \lambda_1 & \lambda_1 & 1 & \lambda_2 \\ \lambda_2 & \lambda_2 & \lambda_2 & 1 \end{pmatrix} \quad (2)$$

in terms of the overlap integrals $\lambda_1 = \int \psi_a \psi_b \, d^3r$ and $\lambda_2 = \int \psi_a \psi_d \, d^3r$ between the bonds. For Eq. (2) to have non-trivial solutions for each eigenenergy E_n ($n = u, v, e_x, e_y$), the following determinant has to be zero,

$$\begin{vmatrix} v_{aa} - E_n & v_{ab} - E_n\lambda_1 & v_{ab} - E_n\lambda_1 & v_{ad} - E_n\lambda_2 \\ v_{ab} - E_n\lambda_1 & v_{aa} - E_n & v_{ab} - E_n\lambda_1 & v_{ad} - E_n\lambda_2 \\ v_{ab} - E_n\lambda_1 & v_{ab} - E_n\lambda_1 & v_{aa} - E_n & v_{ad} - E_n\lambda_2 \\ v_{ab} - E_n\lambda_2 & v_{ab} - E_n\lambda_2 & v_{ab} - E_n\lambda_2 & v_{dd} - E_n \end{vmatrix} = 0 \quad (3)$$

Note that the sites a, b, c are equivalent due to the symmetry of the basal plane. The Coulomb interaction between the sites a and d is roughly equal to that of between a and b, i.e. $|v_{ad}| = (1-\delta)|v_{ab}|$ where $\delta \gtrapprox 0$, since the bond length along the c-axis is only slightly distorted from the basal ones as shown by the density functional theory calculations. Since all sites a-d have carbon atoms, $|v_{dd}| = |v_{aa}| = v_0$. Moreover, the off-site Coulomb interactions are smaller than the on-site interactions, because of the $1/r$ dependence of the electrostatic potentials, which can be expressed as $|v_{ab}| = \epsilon |v_{aa}|$.

Solutions of Eq. (3), with the realistic assumption $\lim \delta \to 0$, leads to the energies of MOs:

$$\begin{aligned} E_u &= -\frac{v_0(\kappa + \Delta\kappa)}{1 + 2\lambda_1 - 3\lambda_2^2}, \\ E_v &= -\frac{v_0(\kappa - \Delta\kappa)}{1 + 2\lambda_1 - 3\lambda_2^2}, \\ E_{e_{x,y}} &= -\frac{v_0(1-\epsilon)}{1-\lambda_1}, \end{aligned} \quad (4)$$

up to $O(\epsilon^2)$. The coefficients κ and $\Delta\kappa$ are given by

$$\begin{aligned} \kappa =& 1 + \lambda_1 + \epsilon(1 - 3\lambda_2), \\ \Delta\kappa =& \big[\lambda_1^2 + 3\lambda_2^2 + \epsilon^2(6\lambda_1 - 6\lambda_2 + 4) \\ &+ \epsilon\left(-6\lambda_1\lambda_2 - 2\lambda_1 + 6\lambda_2^2 - 6\lambda_2\right)\big]^{1/2}, \end{aligned} \quad (5)$$

in terms of the overlap integrals λ_1, λ_2, and the off-site to on-site Coulomb ratio ϵ. In the case of zero overlap between the bonds ($\lambda_1 = \lambda_2 = 0$), according to Eq. (4), the energies E_v and $E_{e_{x,y}}$ become equal, i.e. $E_v = E_{e_{x,y}} = -v_0(1-\epsilon)$ and $E_u = -v_0(1+3\epsilon)$, also indicating that $E_u < E_v$. This can be understood as the defect's asymptotic limit to tetrahedral symmetry.

The true benefit of the above treatment is realized once it is used in conjunction with the energies calculated by DFT. By using the MO energies obtained by DFT (Fig.2) in Eq. (4), we find the previously unknown overlap integrals, the on-site potential energy and the Coulomb ratio of the defect to be $\lambda_1 = 0.0034$, $\lambda_2 = 0.054$, $v_0 = 1.177$eV, and $\epsilon = 0.285$, respectively. Furthermore,

we calculate the eigenfunctions satisfying Eq. (3) as,

$$\begin{aligned} u &= \alpha_u(a+b+c) + \beta_u d, \\ v &= \alpha_v(a+b+c) + \beta_v d, \\ e_x &= \alpha_x(2c-a-b), \\ e_y &= \alpha_y(a-b), \end{aligned} \tag{6}$$

with the coefficients obtained as $\alpha_u = 0.523$, $\beta_u = 0.423$, $\alpha_v = -0.272$, $\beta_v = 0.882$, $\alpha_x = 0.408$, and $\alpha_y = 0.707$. The coefficients of u and v only slightly differ from the readily known coefficients of T_d symmetry [5], i.e. $\alpha_u = \beta_u = 0.5$, $\alpha_v = -0.289$, and $\beta_v = 0.866$. Later on, we use these coefficients to estimate the zero-field splitting of the ground state leading to a remarkable agreement with the experimentally measured values.

Energy order of the doublets

Due to the many-particle nature of the doublets, we cannot obtain the ordering of the states using DFT, which is an effective single-particle description of the system. Therefore, we analyzed the ordering via Coulomb Hamiltonian $H_c = \sum h_i + \sum_{i,j} V_{ee}(r_i, r_j)$ using the wave functions of the states $\Psi^i_{\text{d1-d5}}$ given in Table. I of the main text. One electron (hole) Coulomb terms are included in h_i, whereas $V_{ee}(r_i, r_j) = e^2/(4\pi\epsilon_0|r_i - r_j|)$ is the two-particle Coulomb repulsion potential. Eigen values of h_i in MOs basis are represented by χ and can be estimated from DFT. Many-particle Coulomb integrals are given as $j^0_{ll} = \int \rho_{ll}(1) V_{ee} \rho_{ll}(2) d^3r_1 d^3r_2$, $j_{lm} = \int \rho_{ll}(1) V_{ee} \rho_{mm}(2) d^3r_1 d^3r_2$, and $k_{lm} = \int \rho_{lm}(1) V_{ee} \rho_{lm}(2) d^3r_1 d^3r_2$. The integrals j^0_{ll}, j_{lm}, and k_{lm} are the one-center Coulomb integral, two-particle Coulomb repulsion direct and exchange integrals, respectively. Charge density is defined as $\rho_{lm}(i) = \psi_l(i)^* \psi_m(i)$ belonging to the i^{th} particle in the basis of sp^3 hybridized dangling bond wave functions with $l, m = \{a, b, c, d\}$ and $l \neq m$. We obtain the Coulomb energies of doublets as,

$$\mathrm{E}^E_{e^3} = \chi_{e^3} + 0.67 j^0_{aa} + 2.33 j_{ab} - 0.33 k_{ab} \tag{7}$$

$$\mathrm{E}^{A_2}_{ve^2} = \chi_{ve^2} + 0.22 j^0_{aa} + 1.22 j_{ab} + 1.56 j_{ad} - 1.22 k_{ab} + 0.78 k_{ad} \tag{8}$$

$$\mathrm{E}^E_{ve^2} = \chi_{ve^2} + 0.41 j^0_{aa} + 1.04 j_{ab} + 1.56 j_{ad} - 0.04 k_{ab} - 0.78 k_{ad} \tag{9}$$

$$\mathrm{E}^{A_1}_{ve^2} = \chi_{ve^2} + 0.74 j^0_{aa} + 0.70 j_{ab} + 1.56 j_{ad} + 1.30 k_{ab} - 0.78 k_{ad} \tag{10}$$

$$\mathrm{E}^E_{v^2e} = \chi_{v^2e} + 0.09 j^0_{aa} + 0.61 j^0_{dd} + 0.40 j_{ab} + 1.90 j_{ad} - 0.30 k_{ab} - 0.89 k_{ad} \tag{11}$$

where the relationship $\chi \gg j^0 \gg j \gg k$ holds and due to the nearly T_d symmetry of the center charge localization on the basal and z-axis carbon atoms are assumed to be similar, i.e., $j^0_{aa} \simeq j^0_{dd}$. Furthermore, we obtain the ground state energy in a similar way:

$$\mathrm{E}_g = 1.44(j_{ab} - k_{ab}) + 1.56(j_{ad} - k_{ad}). \tag{12}$$

Assuming $\chi_{v^2e} > \chi_{ve^2} > \chi_{e^3}$, the ordering of doublets becomes $\mathrm{E}^E_{e^3}$, $\mathrm{E}^{A_2}_{ve^2}$, $\mathrm{E}^E_{ve^2}$, $\mathrm{E}^{A_1}_{ve^2}$, and $\mathrm{E}^E_{v^2e}$ increasing in energy.

THREE-PARTICLE STATES

Because of the near-degeneracy of state v with states e_x and e_y, it is energetically favorable for two electrons to occupy the e states instead of paying the energetic cost of doubly occupying the only slightly lower in energy state v. As a result, in the ground state the occupied states are v, e_x and e_y, in the three-hole picture.

For the ve^2 ground state, the three hole configuration space is spanned by 32 ($2 \otimes 4 \otimes 4$) basis functions in the form of single particle Kronecker products $f^j_\kappa = (\{v\} \otimes \{\alpha, \beta\}) \otimes (\{e_x, e_y\} \otimes \{\alpha, \beta\}) \otimes (\{e_x, e_y\} \otimes \{\alpha, \beta\})$. However, consideration of the Pauli exclusion principle discards 8 of them leaving 24 basis states.

Moreover, the single particle irreducible matrix representations for the cases where the degeneracy lies only in the orbital, only in the spin, or in both spaces are simply $\Gamma_E(R) \otimes \mathbb{1}_s$, $\mathbb{1}_o \otimes \Gamma_{E_{1/2}}(R)$, or $\Gamma_E(R) \otimes \Gamma_{E_{1/2}}(R)$, respectively. Note that the identity matrices are defined as $\mathbb{1}_o$ for the orbital and $\mathbb{1}_s$ for the spin subspace. The explicit form of the matrices $\Gamma(R)$ are given in Table I.

R	$\Gamma_E(R)$	$\Gamma_{E_{1/2}}(R)$
$\left\{ \begin{matrix} E \\ \bar{E} \end{matrix} \right\}$	$\begin{bmatrix} 1 & 0 \\ 0 & 1 \end{bmatrix}$	$\pm \begin{bmatrix} 1 & 0 \\ 0 & 1 \end{bmatrix}$
$\left\{ \begin{matrix} C_3^+ \\ \bar{C}_3^+ \end{matrix} \right\}$	$\begin{bmatrix} -\frac{1}{2} & -\frac{\sqrt{3}}{2} \\ \frac{\sqrt{3}}{2} & -\frac{1}{2} \end{bmatrix}$	$\pm \begin{bmatrix} \bar{\epsilon} & 0 \\ 0 & \bar{\epsilon}^* \end{bmatrix}$
$\left\{ \begin{matrix} C_3^- \\ \bar{C}_3^- \end{matrix} \right\}$	$\begin{bmatrix} -\frac{1}{2} & \frac{\sqrt{3}}{2} \\ -\frac{\sqrt{3}}{2} & -\frac{1}{2} \end{bmatrix}$	$\pm \begin{bmatrix} \bar{\epsilon}^* & 0 \\ 0 & \bar{\epsilon} \end{bmatrix}$
$\left\{ \begin{matrix} \sigma_{\nu 1} \\ \bar{\sigma}_{\nu 1} \end{matrix} \right\}$	$\begin{bmatrix} 1 & 0 \\ 0 & -1 \end{bmatrix}$	$\pm \begin{bmatrix} 0 & \bar{1} \\ 1 & 0 \end{bmatrix}$
$\left\{ \begin{matrix} \sigma_{\nu 2} \\ \bar{\sigma}_{\nu 2} \end{matrix} \right\}$	$\begin{bmatrix} -\frac{1}{2} & -\frac{\sqrt{3}}{2} \\ -\frac{\sqrt{3}}{2} & \frac{1}{2} \end{bmatrix}$	$\pm \begin{bmatrix} 0 & \bar{\epsilon}^* \\ \epsilon & 0 \end{bmatrix}$
$\left\{ \begin{matrix} \sigma_{\nu 3} \\ \bar{\sigma}_{\nu 3} \end{matrix} \right\}$	$\begin{bmatrix} -\frac{1}{2} & \frac{\sqrt{3}}{2} \\ \frac{\sqrt{3}}{2} & \frac{1}{2} \end{bmatrix}$	$\pm \begin{bmatrix} 0 & \bar{\epsilon} \\ \epsilon^* & 0 \end{bmatrix}$

TABLE I. Irreducible matrix representations of E and $E_{1/2}$ for orbital and spin degrees of freedom, respectively. $\Gamma_{E_{1/2}}$ is given in helicity basis with $\epsilon = \exp i2\pi/3$.

For the multi-particle ve_xe_y ground state configuration, the irreducible matrix representation $\Gamma^{(j)}_{\lambda\kappa}(R)$ can be decomposed into its orbital and spin components for each particle, i.e. $\Gamma^{(j)}_{\lambda\kappa}(R) = \left[(\mathbb{1} \otimes \Gamma_{E_{1/2}}) \otimes (\Gamma_E \otimes \Gamma_{E_{1/2}}) \otimes (\Gamma_E \otimes \Gamma_{E_{1/2}})\right]^{(j)}_{\lambda\kappa}(R)$. In this form, application of the projection operator [5] on

each basis function,

$$\mathcal{P}^{(j)} f^j_\kappa = (I_j/h) \sum_R \sum_\lambda^{I_j} \chi^{(j)}(R)^* \Gamma^{(j)}_{\lambda\kappa}(R) f^j_\lambda, \qquad (13)$$

yields the symmetry adapted basis functions belonging to the j^{th} representation of the ground state. Character table of $C_{3\nu}$ is given in Table II. This gives us a prescription for generating all the partners of any basis function belonging to a given representation. Further combinations of these symmetry adapted basis functions are then formed according to the spin configurations listed in Table III to finally obtain all the quartet and doublet wave functions of ve^2 configuration listed in Table II of the main text. The wave functions for the *uve* excited state quartet (q2) are also produced in the same way.

	E	C_3^+	C_3^-	$\sigma_{\nu 1}$	$\sigma_{\nu 2}$	$\sigma_{\nu 3}$	$\bar{E}$	$\bar{C}_3^+$	$\bar{C}_3^-$	$\bar{\sigma}_{\nu 1}$	$\bar{\sigma}_{\nu 2}$	$\bar{\sigma}_{\nu 3}$
A_1	1	1	1	1	1	1	1	1	1	1	1	1
A_2	1	1	1	-1	-1	-1	1	1	1	-1	-1	-1
E	2	1	1	0	0	0	2	1	1	0	0	0
$E_{1/2}$	2	1	1	0	0	0	-2	-1	-1	0	0	0
${}^1E_{3/2}$	1	-1	-1	i	i	i	-1	1	1	-i	-i	-i
${}^2E_{3/2}$	1	-1	-1	-i	-i	-i	-1	1	1	i	i	i

TABLE II. Character table of $C_{3\nu}$ double group. 3-particle coordinate (spin) space belongs to the first (last) three rows.

$D^{1/2} \otimes D^{1/2} \otimes D^{1/2}$			
Γ_s	S	m_s	$\psi_S^{m_s}$
$D^{3/2}$	3/2	+3/2	$\|\alpha\alpha\alpha\rangle$
		+1/2	$\|\alpha\alpha\beta\rangle + \|\alpha\beta\alpha\rangle + \|\beta\alpha\alpha\rangle$
		−1/2	$\|\beta\beta\alpha\rangle + \|\beta\alpha\beta\rangle + \|\alpha\beta\beta\rangle$
		−3/2	$\|\beta\beta\beta\rangle$
$D^{1/2}$	1/2	+1/2	$\|\alpha\beta\alpha\rangle - \|\beta\alpha\alpha\rangle$
		−1/2	$\|\beta\alpha\beta\rangle - \|\alpha\beta\beta\rangle$
$D^{1/2}$	1/2	+1/2	$\|\alpha\beta\alpha\rangle + \|\beta\alpha\alpha\rangle - 2\|\alpha\alpha\beta\rangle$
		−1/2	$\|\beta\alpha\beta\rangle + \|\alpha\beta\beta\rangle - 2\|\beta\beta\alpha\rangle$

TABLE III. Free space spin configuration of three holes in terms of spin up α and down β states reduced into irrep. of a quartet $D^{3/2}$ and two doublets $D^{1/2}$.

SPIN-ORBIT ASSISTED TRANSITIONS AMONGST DARK DOUBLET STATES

We show the spin-orbit coupling matrix elements between all doublet manifolds d1−d5 in Table IV using Eq.1 of our manuscript with the symmetry-adapted basis functions given in Table I. The spin-orbit coupling parameters that are perpendicular and parallel to the C_3 axis of the defect are represented by $\lambda_\perp$ and λ_z, respectively. Each element of the matrix is evaluated by $\langle \Psi_i || \mathscr{H}_{SO} || \Psi_j \rangle$ where i and j are the wave functions given as the row and column headings. We also omit the dark doublets, much higher in energy, lying in between the excited quartet states q1 and q2. These will either transition to the lowest excited quartet state (q1) or along the doublet ladder to the five lower doublet states. The key thing to notice here is, as shown in Table IV, all doublet states except d5 have spin-orbit assisted allowed transitions to the lowest d1 doublet. However, d5 doublet can transition to d1 through the other doublets in between and also has strong transition rate -just like d1- into the ground spin $m_s = \pm 3/2$ states by itself which will assist the optical spin polarization process. Therefore, any other high lying doublet states we omitted in this fine structure will follow the general paths shown in our manuscript and will not affect the dominant spin-polarization channel identified as to be through the d1 doublet in our manuscript. Note that d1 is energetically the closest doublet to the ground state (as shown above) and it is also the only one connected to the q1 quartet with a directly allowed spin-orbit assisted transition.

SPIN-SPIN INTERACTION

Spherical tensor components

The spin dipole-dipole operator given in terms of the single particle operators $S_d = \boldsymbol{s}^i \cdot \boldsymbol{s}^j - 3\left(\boldsymbol{s}^i \cdot \hat{\boldsymbol{r}}^{ij}\right)\left(\boldsymbol{s}^j \cdot \hat{\boldsymbol{r}}^{ij}\right)$ can be expressed as $\{A + B + C + D + E + F\}$, using the following spherical tensor components,

$$A = -4\sqrt{\pi/5}\, Y_2^0\, s_z^i s_z^j, \quad B = \sqrt{\pi/5}\, Y_2^0 \left(s_-^i s_+^j + s_+^i s_-^j\right),$$
$$C, D = \mp\sqrt{6\pi/5}\, Y_2^{\mp 1} \left(s_\pm^i s_z^j + s_z^i s_\pm^j\right),$$
$$E, F = -\sqrt{6\pi/5}\, Y_2^{\mp 2} s_\pm^i s_\pm^j. \qquad (14)$$

Orbital parts of A and B terms involving the spherical harmonic Y_2^0 belong to the A_1 symmetry, whereas all other terms belong to the E symmetry. Since the ground state wave functions (Table II of the main text) possess an A_2 orbital symmetry, only A and B terms of Eq. (14) will cause the zero field spin-splitting of the ground state; however, for a q2 excited state with E orbital symmetry and corresponding spin symmetries listed in Table II of the main text, all terms can contribute to the splitting.

We first calculate the matrix elements of S_d for each wave function listed in Table II of the main text by direct evaluation of its spin components. The remaining spatial dependence of the matrix elements can then be analyzed through the Wigner-Eckart theorem using the spatial components of the spherical tensors listed above.

Ground state zero-field spin splitting

In the main text, we report the zero-field spin (ZFS) splitting of the ground state in a compact form as

$$\gamma_g = \gamma_0 \langle \phi^{A_2}_{ve^2} || I_2 || \phi^{A_2}_{ve^2} \rangle / \sqrt{10}, \qquad (15)$$

where I_2 is an irregular solid harmonic of second rank, i.e. $I_l^m = \sqrt{4\pi/(2l+1)} Y_l^m / r^{l+1}$ and $\gamma_0 = \mu_0 g^2 \mu_B^2/(4\pi)$.

	$\Psi^1_{\rm d1}$	$\Psi^2_{\rm d1}$	$\Psi^3_{\rm d1}$	$\Psi^4_{\rm d1}$	$\Psi^1_{\rm d2}$	$\Psi^2_{\rm d2}$	$\Psi^1_{\rm d3}$	$\Psi^2_{\rm d3}$	$\Psi^3_{\rm d3}$	$\Psi^4_{\rm d3}$	$\Psi^1_{\rm d4}$	$\Psi^2_{\rm d4}$	$\Psi^1_{\rm d5}$	$\Psi^2_{\rm d5}$	$\Psi^3_{\rm d5}$	$\Psi^4_{\rm d5}$
$\Psi^1_{\rm d1}$	$-\frac{\lambda_z}{2}$	0	0	0	0	$\frac{-\lambda_\perp}{2\sqrt{3}}$	0	0	0	0	0	$\frac{i\lambda_\perp}{2}$	0	0	0	0
$\Psi^2_{\rm d1}$	0	$-\frac{\lambda_z}{2}$	0	0	$\frac{-\lambda_\perp}{2\sqrt{3}}$	0	0	0	0	0	$\frac{i\lambda_\perp}{2}$	0	0	0	0	0
$\Psi^3_{\rm d1}$	0	0	$\frac{\lambda_z}{2}$	0	0	0	$\frac{-i\lambda_\perp}{2\sqrt{2}}$	$\frac{-i\lambda_\perp}{2\sqrt{2}}$	0	$\frac{-\lambda_\perp}{2}$	0	0	0	0	0	0
$\Psi^4_{\rm d1}$	0	0	0	$\frac{\lambda_z}{2}$	0	0	$\frac{i\lambda_\perp}{2\sqrt{2}}$	$\frac{i\lambda_\perp}{2\sqrt{2}}$	0	$\frac{-\lambda_\perp}{2}$	0	0	0	0	0	0
$\Psi^1_{\rm d2}$	0	$\frac{-\lambda_\perp}{2\sqrt{3}}$	0	0	0	0	0	0	0	0	$\frac{i\lambda_z}{\sqrt{3}}$	0	0	$\frac{-i\lambda_\perp}{2\sqrt{3}}$	0	0
$\Psi^2_{\rm d2}$	$\frac{-\lambda_\perp}{2\sqrt{3}}$	0	0	0	0	0	0	0	0	0	0	$\frac{i\lambda_z}{\sqrt{3}}$	$\frac{i\lambda_\perp}{2\sqrt{3}}$	0	0	0
$\Psi^1_{\rm d3}$	0	0	$\frac{i\lambda_\perp}{2\sqrt{2}}$	$\frac{-i\lambda_\perp}{2\sqrt{2}}$	0	0	0	0	0	0	0	0	0	0	$\frac{-\lambda_\perp}{2\sqrt{2}}$	$\frac{\lambda_\perp}{2\sqrt{2}}$
$\Psi^2_{\rm d3}$	0	0	$\frac{i\lambda_\perp}{2\sqrt{2}}$	$\frac{-i\lambda_\perp}{2\sqrt{2}}$	0	0	0	0	0	0	0	0	0	0	$\frac{-\lambda_\perp}{2\sqrt{2}}$	$\frac{\lambda_\perp}{2\sqrt{2}}$
$\Psi^3_{\rm d3}$	0	0	0	0	0	0	0	0	0	0	0	0	0	0	0	0
$\Psi^4_{\rm d3}$	0	0	$\frac{-\lambda_\perp}{2}$	$\frac{-\lambda_\perp}{2}$	0	0	0	0	0	0	0	0	0	0	$\frac{-i\lambda_\perp}{2}$	$\frac{-i\lambda_\perp}{2}$
$\Psi^1_{\rm d4}$	0	$\frac{-i\lambda_\perp}{2}$	0	0	$\frac{-i\lambda_z}{\sqrt{3}}$	0	0	0	0	0	0	0	0	$\frac{-\lambda_\perp}{2}$	0	0
$\Psi^2_{\rm d4}$	$\frac{-i\lambda_\perp}{2}$	0	0	0	0	$\frac{-i\lambda_z}{\sqrt{3}}$	0	0	0	0	0	0	$\frac{\lambda_\perp}{2}$	0	0	0
$\Psi^1_{\rm d5}$	0	0	0	0	0	$\frac{-i\lambda_\perp}{2\sqrt{3}}$	0	0	0	0	0	$\frac{\lambda_\perp}{2}$	$\frac{\lambda_z}{2}$	0	0	0
$\Psi^2_{\rm d5}$	0	0	0	0	$\frac{i\lambda_\perp}{2\sqrt{3}}$	0	0	0	0	0	$\frac{-\lambda_\perp}{2}$	0	0	$\frac{\lambda_z}{2}$	0	0
$\Psi^3_{\rm d5}$	0	0	0	0	0	0	$\frac{-\lambda_\perp}{2\sqrt{2}}$	$\frac{-\lambda_\perp}{2\sqrt{2}}$	0	$\frac{i\lambda_\perp}{2}$	0	0	0	0	$\frac{-\lambda_z}{2}$	0
$\Psi^4_{\rm d5}$	0	0	0	0	0	0	$\frac{\lambda_\perp}{2\sqrt{2}}$	$\frac{\lambda_\perp}{2\sqrt{2}}$	0	$\frac{i\lambda_\perp}{2}$	0	0	0	0	0	$\frac{-\lambda_z}{2}$

TABLE IV. Spin-orbit matrix elements amongst the dark doublet states. Spin-orbit parameters of the defect are given by λ_z and $\lambda_\perp$ along the C_3 axis and the basal plane of the defect, respectively.

In its open form, it can be written as

$$\gamma_g = \gamma_0 \sqrt{\frac{\pi}{5}} \sum_{i>j} \langle v e_x e_y || \frac{Y^0_{2,ij}}{r^3_{ij}} || v e_x e_y \rangle, \tag{16}$$

where $Y^0_{2,ij}/r^3_{ij}$ can be treated as a pair operator. In terms of the direct and exchange integrals [5, 6], the expectation value of any pair operator F is given by,

$$\begin{aligned} \langle X||F||X\rangle = \sum_{i>j} \{ &\langle a_i a_j | f(i,j) | a_i a_j \rangle \\ &- \langle a_i a_j | f(i,j) | a_j a_i \rangle \}, \end{aligned} \tag{17}$$

where $F = \sum_{i>j} f(i,j)$ is the total pair operator and X is the multi-particle antisymmetrized product (Slater determinant) defined as $AP\left[a_1(1)a_2(2)\cdots a_n(N)\right]$. In the case of ground state ZFS, these are $f(i,j) = Y^0_{2,ij}/r^3_{ij}$ and $X = AP\left[v(1)e_x(2)e_y(3)\right]$.

A quantitative estimate of ZFS splitting can be obtained by switching back to the atomic orbitals,

$$\begin{aligned} \gamma_g &= \langle \Psi^{1,2}_g | \mathcal{H}_S | \Psi^{1,2}_g \rangle_{\pm\frac{3}{2}} - \langle \Psi^{3,4}_g | \mathcal{H}_S | \Psi^{3,4}_g \rangle_{\pm\frac{1}{2}} \\ &= \frac{\gamma_0}{4} \left[\eta_{ad} \langle r^{-3}_{ad} \rangle (1 - 3\cos^2\theta_{ad}) + \eta_{ab} \langle r^{-3}_{ab} \rangle \right], \end{aligned} \tag{18}$$

where the $\eta_{ab} = 1.443$ and $\eta_{ad} = 1.557$ are the respective weight factors of the expectation value $\langle Y^0_{2,ij}/r^3_{ij} \rangle$ originating from total ad and ab pair contributions of MOs after evaluating the determinantal multi-particle wave functions according to Eq. (17) and using the explicit forms of u, v, and $e_{x,y}$ given in Eq. (6). This equation can also be written in a more familiar form starting from the spin dipole-dipole interaction as

$$\gamma_g = \frac{3}{2}\gamma_0 \left\langle \frac{1 - 3\cos^2\theta}{r^3_{ij}} \right\rangle_{\phi^{A\,2}_{ve^2}} \left[S^2_z - \frac{1}{3} S(S+1) \right], \tag{19}$$

where γ_g becomes $D[S^2_z - S(S+1)/3]$. So far we assumed all the charge of unpaired electrons is localized on the neighboring carbon atoms. However, as previously reported [7], only 62.3% of total charge is localized on the neighboring carbon atoms, and this yields to a reduction of roughly $\tau = (1 - (0.377)^2) = 0.858$ in γ_g, i.e. $\gamma_g \to \tau\,\gamma_g$.

Evaluation of Eq. (18) with these weight factors and structure parameters calculated via DFT, i.e. $r_{ab} = 3.3563$Å, $r_{ad} = 3.3567$Å, and $\theta_{ad} = 35.259°$, as well as accounting for the missing charge, results with a ground state ZFS splitting of $2\gamma_g \approx -68$MHz ($D < 0$) for an h-site V^-_{Si} defect in good agreement with the experimentally observed values [8, 9].

LAMBDA SYSTEM

A Λ-type three-level system can be created by a magnetic field transverse to the C_3-axis. Such a field will mix states in the ground and excited manifolds in different ways. This is because in the ground state manifold there is a small spin-spin splitting between states with $|S_z| = 3/2$ and $|S_z| = 1/2$, whereas the corresponding states in the excited manifold are split by the much larger spin-orbit interaction. We assume a weak enough magnetic field such that the coupling of the spin states is

much smaller than the spin-orbit term Δ_e. This allows the eigenstates in the excited manifold to remain in the form shown in the main text (without a B-field). There are several choices for the composition of the Λ system. Below we present some of these options. In all cases, the lower levels are eigenstates of $\hat{S}_x$, which in terms of the states in Table I of the main text are given by

$$\Psi^1_{g,x} \simeq \left[\frac{(1-i)}{4}\Psi^1_{\rm g} + \frac{(1+i)}{4}\Psi^2_{\rm g} + \sqrt{\frac{3}{8}}(\Psi^3_{\rm g} + \Psi^4_{\rm g})\right]$$

$$\Psi^2_{g,x} \simeq \left[-\frac{\sqrt{3}}{4}(1+i)\Psi^1_{\rm g} - \frac{\sqrt{3}}{4}(1-i)\Psi^2_{\rm g} - \frac{1}{\sqrt{8}}(\Psi^3_{\rm g} - \Psi^4_{\rm g})\right]$$

$$\Psi^3_{g,x} \simeq \left[\frac{\sqrt{3}}{4}(1-i)\Psi^1_{\rm g} + \frac{\sqrt{3}}{4}(1+i)\Psi^2_{\rm g} - \frac{1}{\sqrt{8}}(\Psi^3_{\rm g} + \Psi^4_{\rm g})\right]$$

$$\Psi^4_{g,x} \simeq \left[-\frac{(1+i)}{4}\Psi^1_{\rm g} - \frac{(1-i)}{4}\Psi^2_{\rm g} + \sqrt{\frac{3}{8}}(\Psi^3_{\rm g} - \Psi^4_{\rm g})\right],$$

in descending $\langle S_x\rangle$ value, 3/2,1/2,-1/2, -3/2 and where, for simplicity, we have ignored a small correction from the ZFS.

In the first approach for a Λ system we can select states with the same weight of $|\uparrow\uparrow\uparrow\rangle$, e.g., states $\{\Psi^1_{g,x}, \Psi^4_{g,x}\}$ or $\{\Psi^2_{g,x}, \Psi^3_{g,x}\}$. In the excited state manifold then we select Ψ^+_e, which is defined in the main text and has well-defined projection of spin along the z (or C_3) axis, due to the suppression of Zeeman mixing originating from the large SO interaction. The effect is similar to the selection rules in self-assembled quantum dot electron-trion systems under a Voigt B field. Because of this composition of the Lambda system, the polarization of the two transitions is the same. The frequency however is different, and that degree of freedom can be used as the 'handle' with which to the emitted photon can be manipulated.

An alternate scheme for a Λ system is to select as lower levels the eigenstates of $\hat{S}_x$ with eigenvalues -1/2 and 3/2, $\Psi^3_{g,x}$ and $\Psi^1_{g,x}$. In the excited state manifold the relevant state is then $(\Psi^7_{\rm q2} + \Psi^8_{\rm q2})/\sqrt{2}$, i.e., again mixing to the states with different spin projection along z has been ignored in the excited manifold due to the large SO splitting. We note that here the two transitions have the same polarization but, unlike the scheme above, different dipole moments, originating from the different coefficients of $\Psi^3_{\rm g}$, $\Psi^4_{\rm g}$ in the states $\Psi^3_{g,x}$ and $\Psi^1_{g,x}$.

[1] P. Giannozzi, S. Baroni, N. Bonini, M. Calandra, R. Car, C. Cavazzoni, D. Ceresoli, G. L. Chiarotti, M. Cococcioni, I. Dabo, et al., Journal of Physics: Condensed Matter **21**, 395502 (19pp) (2009), URL `http://www.quantum-espresso.org`.

[2] J. P. Perdew and Y. Wang, Phys. Rev. B **33**, 8800 (1986).

[3] J. P. Perdew, K. Burke, and M. Ernzerhof, Phys. Rev. Lett. **77**, 3865 (1996).

[4] E. Hückel, Zeitschrift für Physik **70**, 204 (1931).

[5] M. Tinkham, *Group Theory and Quantum Mechanics* (Dover, New York, 2003).

[6] G. D. Mahan, *Many-particle Physics* (Kluwer Academic, New York, 2000).

[7] N. Mizuochi, S. Yamasaki, H. Takizawa, N. Morishita, T. Ohshima, H. Itoh, and J. Isoya, Phys. Rev. B **66**, 235202 (2002).

[8] H. Kraus, V. A. Soltamov, D. Riedel, S. Väth, F. Fuchs, A. Sperlich, P. G. Baranov, V. Dyakonov, and G. V. Astakhov, Nature Physics **10**, 157 (2014).

[9] S. G. Carter, O. O. Soykal, P. Dev, S. E. Economou, and E. R. Glaser, Phys. Rev. B **92**, 161202(R) (2015).